FRONTIERS OF PHYSICS

RESEARCH ARTICLE
Volume 18 / Issue 5 / 52306 / 2023

Magnetic-field-sensitive multi-wave interference

Wenhua Yan [1], Xudong Ren [1], Wenjie Xu [1,†], Zhongkun Hu [1,2], Minkang Zhou [1]

1 MOE Key Laboratory of Fundamental Physical Quantities Measurements, Hubei Key Laboratory of Gravitation and Quantum Physics, PGMF and School of Physics, Huazhong University of Science and Technology, Wuhan 430074, China

2 Wuhan Institute of Quantum Technology, Wuhan 430206, China

Corresponding author. E-mail: †wenjiexu@hust.edu.cn

Received January 4, 2023; accepted April 12, 2023

ABSTRACT

We report an experimental study of magnetic-field-sensitive multi-wave interference, realized in a three-wave RF-atom system. In the $F = 1$ hyperfine level of the ^{87}Rb $5^2S_{1/2}$ ground state, Ramsey fringes were observed via the spin-selective Raman detection. A decrease in the fringe contrast was observed with increasing free evolution time. The maximum evolution time for observable fringe contrasts was investigated at different atom temperatures, under free-falling and trapped conditions. As the main interest of the Ramsey method, the improvement in magnetic field resolution is observed with an increase of evolution time T up to 3 ms and with the measurement resolution reaching 0.85 nT. This study paves the way for precision magnetic field measurements based on cold atoms.

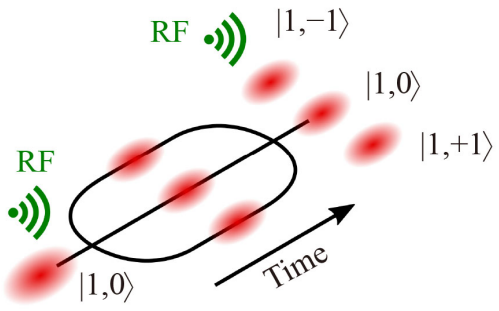

Keywords atom interferometer, magnetometer, cold atom device, multi-wave interference

1 Introduction

Ramsey interference [1] has been widely used in metrology, notably with the principle of atomic fountain clocks [2–4]. The interference fringe pattern in a two-wave system is well-known and can be reversed to determine the physical quantities associated with the phase shift. In multi-wave systems, studies [5–10] have revealed that the interference fringes are distorted and produce higher fringe slopes, which led to improved measurement sensitivity.

An intrinsic atomic system demonstrating multi-wave interference is in the Zeeman effect on alkali atoms, which contains $2F + 1$ spin levels in the hyperfine ground states. Under a magnetic field, both sides of the spin levels beside $m_F = 0$ move in opposite directions, making the multilevel structure sensitive to the magnetic field. By applying radio frequency (RF) fields to couple the spin levels, multi-wave interference fringes sensitive to magnetic fields can be implemented.

A straightforward application for this is magnetic field sensing. Different types of atomic magnetometers such as DRAM [11], CPT [12, 13] and SERF [14] have high sensitivity levels exceeding $\mathrm{pT}/\sqrt{\mathrm{Hz}}$ and even $\mathrm{fT}/\sqrt{\mathrm{Hz}}$. More detailed reviews of atomic and other various magnetometers can be found in Refs. [15, 16]. They have demonstrated state-of-the-art results in terms of sensitivity, spatial resolution, dimension, etc.

The evaluation of the systematic errors that are induced by magnetic fields in some atom interferometry experiments, such as those involving atomic clocks [17–19], gravimeters [20–23], gyroscopes [24–26] and short-range forces measurements [27–30], is important. In these scenarios, the use of the aforementioned magnetometers is inconvenient owing to the necessity of measuring the magnetic field at the position of the atoms inside a scientific vacuum chamber. Therefore, the research of magnetic field measurements based on

Higher Education Press

https://doi.org/10.1007/s11467-023-1300-8

Ramsey interference [17, 31], which can be applied *in situ*, provides a method or reference in this context.

The merit of the Ramsey method lies in improving measurement sensitivity by increasing the free evolution time. This feature has been validated on atomic clocks [2–4]. Besides, in contrast to the Raman transition coupling [10, 18, 31], RF coupling is used to avoid light shift. In this article, we report the experimental study of multi-wave interference. As a demonstration, the multi-wave interference in a gravimeter based on an ultracold atom source [32] was observed.

The article is arranged as follows. In Section 2, we provide the necessary theoretical expressions for the experiment. In Section 3, a summary of the experimental apparatus is presented. In Section 4, we present the results. Finally, the discussion and conclusions are presented.

2 Theory

We use the three spin levels in the $F = 1$ hyperfine ground state of $^{87}\mathrm{Rb}\,5^2\mathrm{S}_{1/2}$ to demonstrate multi-wave Ramsey interference. When the atoms are under a static magnetic field $\boldsymbol{B}$, the energy gaps between Zeeman levels are $|-\boldsymbol{\mu}\cdot\boldsymbol{B}|$. We couple the spin states with RF radiation in the form of Eq. (1).

$$\boldsymbol{B}_{\mathrm{RF}} = B_0 \boldsymbol{e}_{\mathrm{RF}} \cos(\omega t + \varphi), \tag{1}$$

where B_0 is the RF waveform amplitude, $\boldsymbol{e}_{\mathrm{RF}}$ indicates the polarization, ω is the RF circular frequency, and φ is the RF initial phase. The RF detuning is

$$\delta = \omega - \frac{|-\boldsymbol{\mu}\cdot\boldsymbol{B}|}{\hbar} = \omega - \frac{\mu_{\mathrm{B}} B}{2\hbar}, \tag{2}$$

where μ_{B} is the Bohr magneton.

The evolution of the system is the solution to the rotating wave approximated Schrödinger equation

$$\mathrm{i}\hbar\dot{\boldsymbol{c}} = \boldsymbol{H}\boldsymbol{c}, \tag{3}$$

where $\boldsymbol{H}$ is the Hamiltonian

$$\boldsymbol{H} = \hbar \begin{pmatrix} -\delta & \sqrt{2}\Omega \mathrm{e}^{\mathrm{i}\varphi} & 0 \\ \sqrt{2}\Omega \mathrm{e}^{-\mathrm{i}\varphi} & 0 & \sqrt{2}\Omega \mathrm{e}^{\mathrm{i}\varphi} \\ 0 & \sqrt{2}\Omega \mathrm{e}^{-\mathrm{i}\varphi} & \delta \end{pmatrix}, \tag{4}$$

$\boldsymbol{c} = (c_1, c_2, c_3)^{\mathrm{T}}$ is the state vector containing the amplitudes for $|F = 1, m_F = -1\rangle$, $|1, 0\rangle$ and $|1, +1\rangle$ spin states, Ω is the Rabi frequency quantifying the coupling strength. The details of the Hamiltonian, Eq. (4), the corresponding deduced time evolution operator $\boldsymbol{U}$ and the level scheme can be found in Ref. [33], where the effective Rabi frequency $\Omega_{\mathrm{eff}} = \sqrt{\delta^2 + 4\Omega^2}$.

The Ramsey sequence consists of two RF pulses with duration τ and a period of evolution time T, as shown in Fig. 1. During the evolution, considering the RF and magnetic field induced phase, the free time evolution operator $\boldsymbol{U}_f$ is

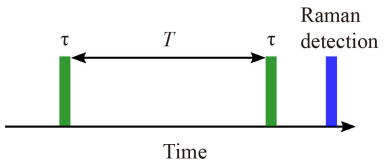

Fig. 1 Experimental sequence of the Ramsey interference in the three-wave system. Raman spin-selective detection is used to read the population in spin states.

$$\boldsymbol{U}_f = \begin{pmatrix} \mathrm{e}^{\mathrm{i}\delta T} & 0 & 0 \\ 0 & 1 & 0 \\ 0 & 0 & \mathrm{e}^{-\mathrm{i}\delta T} \end{pmatrix}. \tag{5}$$

Setting the initial state at time $t = 0$ as $\boldsymbol{c}(0)$, the final state of the Ramsey interferometer is

$$\boldsymbol{c}(T + 2\tau) = \boldsymbol{U}(\tau)\boldsymbol{U}_f(T)\boldsymbol{U}(\tau)\boldsymbol{c}(0). \tag{6}$$

Setting $\tau = \pi/(4\Omega_{\mathrm{eff}})$ and $\boldsymbol{c}(0) = (0, 1, 0)^{\mathrm{T}}$, after the Ramsey sequence, the probabilities of the $|1, 0\rangle$ and $|1, \pm 1\rangle$ states are given as Eqs. (7) and (8), respectively.

$$P_0(\phi) = \frac{1}{4}(1 - \cos\phi)^2, \tag{7}$$

where the phase shift $\phi = \delta T$,

$$P_{\pm 1}(\phi) = \frac{1}{8}(1 + \cos\phi)(3 - \cos\phi). \tag{8}$$

3 Experimental apparatus

The three-wave Ramsey interference magnetometer is integrated into a reported BEC gravimeter [32]. The diameter of the lab-made RF coil is 40 mm, and the number of turns is 30. To avoid the Titanium vacuum chamber blocking the propagation of the RF field, the RF coil must be put near the viewports of the gravimeter, as shown in Fig. 2.

The distance between the center of the RF coil and the atomic cloud is 78(5) mm. According to the relationship between the magnetic dipole matrix element and the desired Rabi frequency [34], an RF field oscillating with an amplitude of 0.7 mG is estimated to achieve a Rabi frequency of $2\pi \times 980$ Hz. The target B field at the location of the atomic cloud is ~ 60 mG, corresponding to the Zeeman energy gap of ~ 42 kHz.

The direction of the B field is along the z-axis in Fig. 2. The RF field diffusion and the hindrance of propagation from the metal vacuum chamber cause difficulty in the alignment of the RF coil, compared to the situation with laser optics. Thus, the RF coil orientation near the viewports was manually adjusted so that the Rabi oscillation

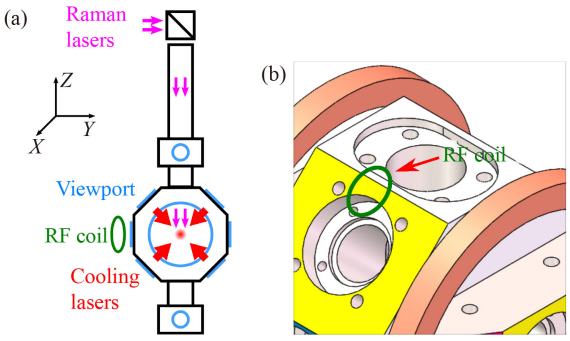

Fig. 2 **(a)** Global view and **(b)** detailed view of the atomic interference magnetometer integrated into a BEC gravimeter.

could be optimized. Through this, the RF system was properly deployed.

At the end of the interferometer sequence, we used the Raman transition of $\Delta F = +1$, $\Delta m_F = 0$ to transfer the atoms from a specific spin state in $F = 1$ to $F = 2$ and then counted the atom numbers in $F = 1$ and $F = 2$ states as N_1 and N_2 with resulting probability $P' = N_1/(N_1 + N_2)$. Considering the Raman two-photon efficiency η in the experiment, the normalized probability was $P = P'/\eta$. The same process can be applied to obtain the probability of $|1, \pm 1\rangle$ state.

4 Results

First, the initial state $|1, 0\rangle$ was prepared. Doppler cooling, polarization gradient cooling, loading into the optical cross dipole trap (OCDT), and evaporation cooling to atoms' temperature of 500 nK are performed as reported in Ref. [32]. By the Raman spectroscopy shown in Fig. 3, three Gaussian peaks were obtained with amplitudes P'_{-1}, P'_0, and P'_{+1} representing the populations in $|1, -1\rangle$, $|1, 0\rangle$, and $|1, +1\rangle$ states without normalization. For detection of

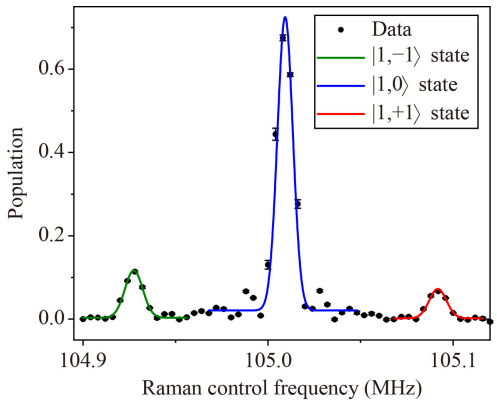

Fig. 3 Raman spectrum of the initial state. Solid lines are the Gaussian fits representing the relative ratio in the spin states.

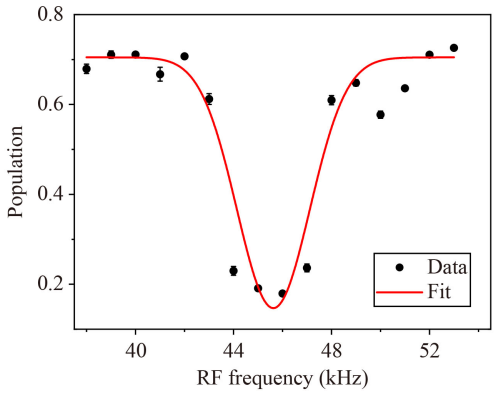

Fig. 4 RF frequency scan for the resonant transition frequency.

the $|1, 0\rangle$ state, the Raman efficiency η was estimated by

$$\eta = P'_{-1} + P'_0 + P'_{+1}. \quad (9)$$

By this means of estimation, the Raman efficiency in the three spin states is assumed to be the same. From Fig. 3, $\eta = 88(5)\%$. This value was used for normalization in the article.

Free-falling atomic clouds were used in the experiment. The quantization B field was approximately 60 mG in the region with a falling time of less than 10 ms. We scanned the RF frequency using single pulses to get the resonance curve shown in Fig. 4. The center of the Gaussian fit indicated a resonant frequency of 45.5 kHz. At this frequency, we spanned the RF pulse duration to get the Rabi oscillation of the $|1, 0\rangle$ state, as shown in Fig. 5. With the exponentially decaying cosine fit, the first population inversion occurred at 0.29 ms. The effective Rabi frequency Ω_{eff} was deduced as $2\pi \times [1/(4 \times 0.29\ \text{ms})] = 2\pi \times 864$ Hz. We set $\tau = 0.14$ ms for the next-step Ramsey sequence.

With a fixed B field, by changing the RF frequency ω during the free evolution time T, the phase shift ϕ can be scanned to produce interference fringes. We set the free evolution time $T = 0.4$ ms to extract Ramsey fringes in the three spin states, as shown in Fig. 6. From the fit to Eqs. (7) and (8), the phase behavior in $|1, \pm 1\rangle$ is reversed compared to that of the $|1, 0\rangle$ state with half the amplitude.

To determine the fringe center, we observed the Ramsey fringes with different evolution times. The overlapping fringe centers in Fig. 7 reveal the amplitude of the B field.

We further increased the evolution time T to observe the fringes shown in Fig. 8. The contrast decreased with increasing T. When $T = 3$ ms, the fringe contrast was about 33%, and the fringes still could be fit. At evolution times of 6 and 9 ms, the contrast decreased to less than 20%, and the fit was close to the range of the error bars.

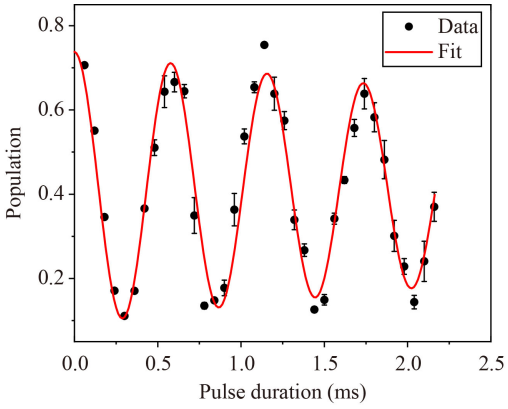

Fig. 5 Rabi oscillation initialized and observed in $|1,0\rangle$ state.

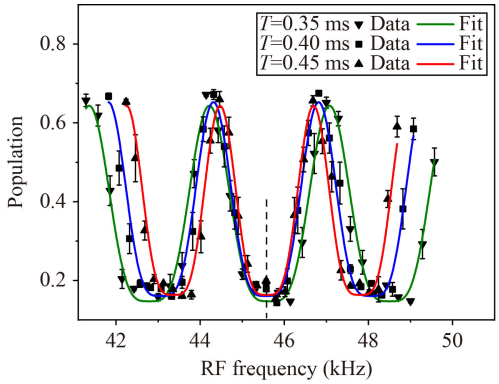

Fig. 7 Ramsey fringes with different evolution times. The dashed line indicates the overlapped fringe center.

This is because, with increasing evolution time under the free-falling condition, the effect of the magnetic field gradient becomes significant. The B field gradient in space behaves as magnetic field variations over time during the interferometer sequence. The variation of the B field is the most likely reason for the dephasing of the interferometer, presented as the vanishing of the fringe contrast, which is also pointed out in Ref. [5]. In the worst case, the second RF pulse will be out of resonance with increases of T or B field variation.

The finite temperature of the atomic cloud, combined with the B field gradient, is an important factor in the fringe contrast decay. Because of the temperature of the atoms, the atomic cloud expands during free fall. With the B field gradient, each atom experiences a different variation in B over time during the Ramsey sequence. The fringe contrast will decrease and be washed out if the atomic cloud is too hot.

We observed fringe contrast in different atom temperatures under free-falling condition, as shown in Fig. 9. Overall, the fitted exponential decay time T_D that characterizes the maximum free evolution time increased with decreasing atom temperature. The lower the atom temperature, the smaller the atomic cloud was during free fall. The critical temperature of the BEC transition was 200 nK. Above the critical temperature, the estimated evolution time was approximately 6 ms. At 100 nK, the estimated evolution time of 35.5 ms was due to the even slower expansion of the BEC. The experiment was conducted for the longest falling time of 20 ms; therefore, the 35.5 ms here demonstrates the estimation.

Furthermore, we observed the fringe contrasts for atoms trapped in the OCDT, as shown in Fig. 10. Without the expansion of the atomic cloud, the free evolution time was drastically increased to the order of 500 ms. This was also true under the free-falling condition; the estimated evolution time increased with decreasing atom

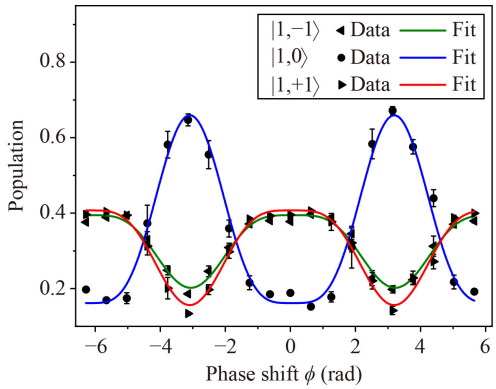

Fig. 6 Interference fringes observed on the three spin states.

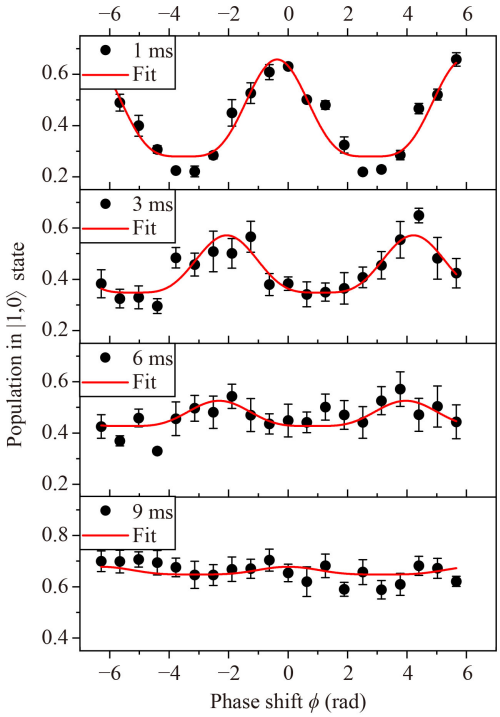

Fig. 8 Fringes with the increase of evolution time.

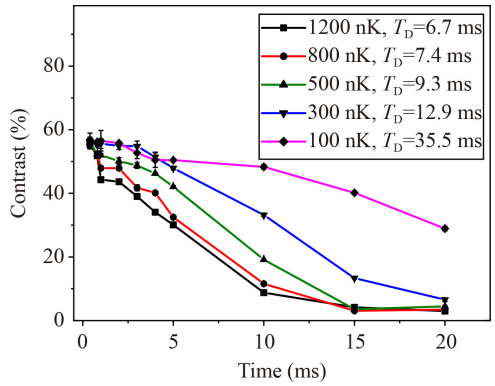

Fig. 9 Fringe contrast decay with different temperatures of atoms under free falling condition.

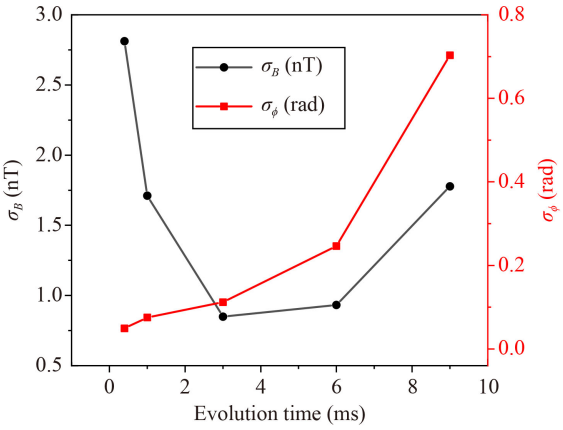

Fig. 11 Phase resolution σ_ϕ and magnetic field resolution σ_B in different evolution time T.

temperature. However, under free-fall condition, even when the fringe contrast held for a long time, the fringe was not useful for fitting. When atoms were trapped in the OCDT, because of the spin-dependent interaction [9, 35–41] that may redistribute spin populations, the phase of the interferometer was out of order.

By characterizing the measurement resolution using the standard error of the mean from the fitted fringes with an integration time of 411 s (for 100 shots), the resolution of the interferometer phase σ_ϕ and B field σ_B with different evolution times were summarized, as shown in Fig. 11. Because of the relationship $\sigma_B/\sigma_\phi = 2\hbar/(\mu_B T)$, although the phase resolution worsens with increasing free evolution time T, the magnetic field resolution improves until T reaches 3 ms, indicating 0.85 nT. This is a clear demonstration of the advantage of the Ramsey interference method.

5 Discussion

The demonstrated experimental results and the deduction of Eq. (7) are for cases with strong driving condition such that the RF pulses are near-resonant. This is to

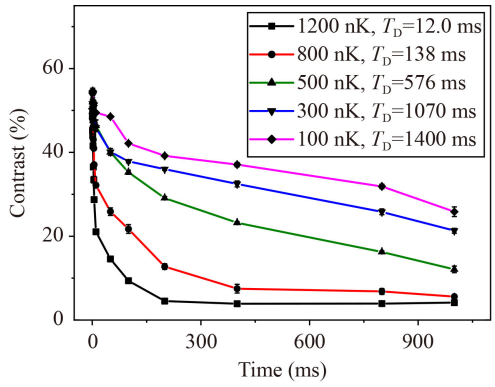

Fig. 10 Fringe contrast decay with different temperatures of atoms under OCDT trapped condition.

expand the overall envelope of the Ramsey fringe, which arises from some effects that make the response of the atoms non-resonant, such as the atom temperature or variations in the B field. During the experiment, there was no spatial separation of atomic clouds, so $\Omega_{\text{eff}}\tau$ could be any value except π to produce fringes. The fringe slope produced by $\pi/4$ pulses is 0.66 rad^{-1}, higher than 0.5 rad^{-1} in a typical Ramsey two-wave system. Our goal is to perform measurements with $\pi/2$ pulses in a three-wave system, producing a fringe slope of 1.0 rad^{-1}, which leads to the highest theoretical measurement sensitivity. However, the sensitivity to B field variations in time will become higher as well. The origin of the variations is primarily the low-frequency ambient magnetic field noise and the noise of the electric current-produced B field.

Currently, there is no magnetic shield or magnetic field stabilization [42, 43] in the experimental apparatus. The demonstrated result of this work is not competitive with those of the developed magnetometers [11–14] or even with the measurement of the magnetic field inside a vacuum chamber [19, 31], possibly due to the magnetic field gradient. As pointed out in Ref. [5] and calculated in Ref. [33], magnetic field gradients may cause dephasing of the interferometer, which results in decreased sensitivity. A magnetic shield may reduce the magnetic field gradient and the environmental magnetic field noise. Magnetic field stabilization [42, 43] can further suppress magnetic field noise, leading to improved results. Besides, notably, Ref. [18] measured magnetic field vector and Ref. [17] presented a more rigorous analysis of the Ramsey method.

From Figs. 9 and 10, the benefit of using a colder atom source is clear. However, evaporation cooling sacrifices atom numbers for lower atom temperatures. Therefore, the resolution limited by the number of atoms under the context of standard quantum limit [44] will worsen. This is the trade-off between atom temperature and the atom number.

With the free-falling configuration, the limit for the

free evolution time T depends on the available falling distance. The dephasing caused by the magnetic field gradient and the atom temperature is calculated in Ref. [33]. Last but not least, according to Ref. [45], the decomposition of the oscillating RF field $\boldsymbol{B}_{\mathrm{RF}}$ parallel and perpendicular to the B field cause energy shifts, which will lead to systematic errors. The next step for improvement requires consideration of the discussed elements.

6 Conclusion

In conclusion, we have presented experimental results of multi-wave interference, driven by separated RF pulses, in a three-wave RF-atom system. The initial state was the $|1,0\rangle$ state. The Rabi oscillation showed an RF-atom coupling strength of 864 Hz. Spin-selective detection was carried out by Raman transition to observe the interference fringes in the $|1,0\rangle$ state. Overlapped fringe centers with different evolution times indicated the absolute value of the magnetic field. The effect of atomic cloud expansion was investigated using fringe contrast as a function of evolution time. Under the free-falling condition, evolution time with an observable fringe contrast reached approximately 10 ms with atomic clouds of 300 nK. When atoms were trapped in the OCDT, this value reached 1 s. Finally, a gain in the measured magnetic field resolution σ_B was observed with an increase of evolution time until T reaches 3 ms, which demonstrates a measurement resolution of 0.85 nT. This work paves the way for precision magnetic field measurement through the reported scheme. Next-step analyses of noise sources and the fine-tuning of experimental conditions are underway.

Acknowledgements This study was supported by the National Key Research and Development Program of China (Grant No. 2020YFC2200200), the National Natural Science Foundation of China (Grants Nos. 12004128, 12104174, and 12274163), and Open Fund of Wuhan, Gravitation and Solid Earth Tides, National Observation and Research Station (Grants Nos. WHYWZ202211 and WHYWZ202104). We thank Dr. Xiaochun Duan and Dr. Jean-Michel Le Floch for the enlightening talk about this work. Codes and data are available upon request from the authors. The authors declare no conflicts of interest.

Appendix

The evolution of states under RF radiation of pulse duration τ is given by Eq. (10). The Rabi oscillation in the $|1,0\rangle$ and $|1,\pm1\rangle$ states are given by Eqs. (11) and (12), respectively,

$$\boldsymbol{c}(\tau) = \boldsymbol{U}(\tau)\boldsymbol{c}(0), \tag{10}$$

$$P_{\mathrm{Rabi},0} = \frac{1}{2}[1+\cos(2\Omega_{\mathrm{eff}}\tau)], \tag{11}$$

$$P_{\mathrm{Rabi},\pm1} = \frac{1}{4}[1-\cos(2\Omega_{\mathrm{eff}}\tau)]. \tag{12}$$

The first full population inversion occurs when $\Omega_{\mathrm{eff}}\tau = \pi/2$. Under this configuration, a $\pi/4$ pulse where $\Omega_{\mathrm{eff}}\tau = \pi/4$ makes the population one half in $|1,0\rangle$ state and one quarter in the $|1,\pm1\rangle$ states, like a so-called "$\pi/2$" pulse in a two-level system.

References

1. N. F. Ramsey, A molecular beam resonance method with separated oscillating fields , *Phys. Rev.* 78(6), 695 (1950)
2. T. P. Heavner, E. A. Donley, F. Levi, G. Costanzo, T. E. Parker, J. H. Shirley, N. Ashby, S. Barlow, and S. R. Jefferts, First accuracy evaluation of NIST-F2, *Metrologia* 51(3), 174 (2014)
3. J. Guena, M. Abgrall, D. Rovera, P. Laurent, B. Chupin, M. Lours, G. Santarelli, P. Rosenbusch, M. E. Tobar, Ruoxin Li, K. Gibble, A. Clairon, and S. Bize, Progress in atomic fountains at LNE-SYRTE, *IEEE Trans. Ultrason. Ferroelectr. Freq. Control* 59(3), 391 (2012)
4. V. Gerginov, N. Nemitz, S. Weyers, R. Schröder, D. Griebsch, and R. Wynands, Uncertainty evaluation of the caesium fountain clock PTB-CSF2, *Metrologia* 47(1), 65 (2010)
5. M. Sadgrove, Y. Eto, S. Sekine, H. Suzuki, and T. Hirano, Ramsey interferometry using the Zeeman sublevels in a spin-2 Bose gas, *J. Phys. Soc. Jpn.* 82(9), 094002 (2013)
6. L. Chen, K. Zhang, Y. Xu, Q. Luo, W. Xu, M. Zhou, and Z. Hu, Multi-wave atom interferometer based on Doppler-insensitive Raman transition, *Opt. Express* 28(6), 8463 (2020)
7. Petrovic, I. Herrera, P. Lombardi, F. Schäfer, and F. S. Cataliotti, A multi-state interferometer on an atom chip, *New J. Phys.* 15(4), 043002 (2013)
8. M. Robert-de-Saint-Vincent, J. P. Brantut, C. J. Bordé, A. Aspect, T. Bourdel, and P. Bouyer, A quantum trampoline for ultra-cold atoms, *Europhys. Lett.* 89(1), 10002 (2010)
9. M. Gustavsson, E. Haller, M. J. Mark, J. G. Danzl, R. Hart, A. J. Daley, and H. C. Nägerl, Interference of interacting matter waves, *New J. Phys.* 12(6), 065029 (2010)
10. M. K. Zhou, K. Zhang, X. C. Duan, Y. Ke, C. G. Shao, and Z. K. Hu, Atomic multiwave interferometer for Aharonov–Casher-phase measurements, *Phys. Rev. A* 93(2), 023641 (2016)
11. G. Di Domenico, H. Saudan, G. Bison, P. Knowles, and A. Weis, Sensitivity of double-resonance alignment magnetometers, *Phys. Rev. A* 76(2), 023407 (2007)
12. S. Knappe, P. D. D. Schwindt, V. Gerginov, V. Shah, L. Liew, J. Moreland, H. G. Robinson, L. Hollberg, and J. Kitching, Microfabricated atomic clocks and magnetometers, *J. Opt. A* 8(7), S318 (2006)
13. P. D. D. Schwindt, S. Knappe, V. Shah, L. Hollberg, J. Kitching, L. A. Liew, and J. Moreland, Chip-scale

atomic magnetometer, *Appl. Phys. Lett.* 85(26), 6409 (2004)
14. J. Li, W. Quan, B. Zhou, Z. Wang, J. Lu, Z. Hu, G. Liu, and J. Fang, SERF atomic magnetometer – recent advances and applications: A review, *IEEE Sens. J.* 18(20), 8198 (2018)
15. D. Budker and M. Romalis, Optical magnetometry, *Nat. Phys.* 3(4), 227 (2007)
16. M. W. Mitchell and S. P. Alvarez, Quantum limits to the energy resolution of magnetic field sensors, *Rev. Mod. Phys.* 92(2), 021001 (2020)
17. W. Zhao, W. Qian, D. Lv, and R. Wei, Improvement of average magnetic field measurement based on magnetic-field-sensitive Ramsey fringes, *Opt. Lett.* 47(8), 2073 (2022)
18. W. Wang, R. Dong, R. Wei, J. Lin, F. Zou, T. Chen, and Y. Wang, Measuring magnetic field vector by stimulated Raman transitions, *Appl. Phys. Lett.* 108(12), 122401 (2016)
19. C. Shi, R. Wei, Z. Zhou, D. Lv, T. Li, and Y. Wang, Magnetic field measurement on ^{87}Rb atomic fountain clock, *Chin. Opt. Lett.* 8, 549 (2010)
20. A. Peters, K. Y. Chung, and S. Chu, High-precision gravity measurements using atom interferometry, *Metrologia* 38(1), 25 (2001)
21. Z. K. Hu, B. L. Sun, X. C. Duan, M. K. Zhou, L. L. Chen, S. Zhan, Q. Z. Zhang, and J. Luo, Demonstration of an ultrahigh-sensitivity atom-interferometry absolute gravimeter, *Phys. Rev. A* 88(4), 043610 (2013)
22. Z. Y. Wang, T. Chen, X. L. Wang, Z. Zhang, Y. F. Xu, and Q. Lin, A precision analysis and determination of the technical requirements of an atom interferometer for gravity measurement, *Front. Phys. China* 4(2), 174 (2009)
23. J. Wang, L. Zhou, R. B. Li, M. Liu, and M. S. Zhan, Cold atom interferometers and their applications in precision measurements, *Front. Phys. China* 4(2), 179 (2009)
24. R. Gautier, M. Guessoum, L. A. Sidorenkov, Q. Bouton, A. Landragin, and R. Geiger, Accurate measurement of the Sagnac effect for matter waves, *Sci. Adv.* 8(23), eabn8009 (2022)
25. W. J. Xu, L. Cheng, J. Liu, C. Zhang, K. Zhang, Y. Cheng, Z. Gao, L. S. Cao, X. C. Duan, M. K. Zhou, and Z. K. Hu, Effects of wave-front tilt and air density fluctuations in a sensitive atom interferometry gyroscope, *Opt. Express* 28(8), 12189 (2020)
26. Z. W. Yao, S. B. Lu, R. B. Li, J. Luo, J. Wang, and M. S. Zhan, Calibration of atomic trajectories in a large-area dual-atom-interferometer gyroscope, *Phys. Rev. A* 97(1), 013620 (2018)
27. X. Alauze, A. Bonnin, C. Solaro, and F. P. D. Santos, A trapped ultracold atom force sensor with a μm-scale spatial resolution, *New J. Phys.* 20(8), 083014 (2018)
28. R. Bennett and D. H. J. O'Dell, Revealing short-range non-Newtonian gravity through Casimir–Polder shielding, *New J. Phys.* 21(3), 033032 (2019)
29. P. Wolf, P. Lemonde, A. Lambrecht, S. Bize, A. Landragin, and A. Clairon, From optical lattice clocks to the measurement of forces in the Casimir regime, *Phys. Rev. A* 75(6), 063608 (2007)
30. S. Dimopoulos and A. A. Geraci, Probing submicron forces by interferometry of Bose–Einstein condensed atoms, *Phys. Rev. D* 68(12), 124021 (2003)
31. X. B. Deng, Y. Y. Xu, X. C. Duan, and Z. K. Hu, Precisely mapping the absolute magnetic field in vacuum by an optical ramsey atom interferometer, *Phys. Rev. Appl.* 15(5), 054062 (2021)
32. H. Zhang, X. Ren, W. Yan, Y. Cheng, H. Zhou, Z. Gao, Q. Luo, M. Zhou, and Z. Hu, Effects related to the temperature of atoms in an atom interferometry gravimeter based on ultra-cold atoms, *Opt. Express* 29(19), 30007 (2021)
33. W. Yan, X. Ren, M. Zhou, and Z. Hu, Precision magnetic field sensing with dual multi-wave atom interferometer, *Sensors (Basel)* 23(1), 173 (2022)
34. F. Reinhard, Design and construction of an atomic clock on an atom chip, Thesis, Université Pierre et Marie Curie-Paris VI, 2009
35. Y. Eto, M. Sadgrove, S. Hasegawa, H. Saito, and T. Hirano, Control of spin current in a Bose gas by periodic application of π pulses, *Phys. Rev. A* 90(1), 013626 (2014)
36. M. Fattori, C. D'Errico, G. Roati, M. Zaccanti, M. Jona-Lasinio, M. Modugno, M. Inguscio, and G. Modugno, Atom interferometry with a weakly interacting Bose–Einstein condensate, *Phys. Rev. Lett.* 100(8), 080405 (2008)
37. M. Fattori, T. Koch, S. Goetz, A. Griesmaier, S. Hensler, J. Stuhler, and T. Pfau, Demagnetization cooling of a gas, *Nat. Phys.* 2(11), 765 (2006)
38. S. Hensler, A. Greiner, J. Stuhler, and T. Pfau, Depolarisation cooling of an atomic cloud, *Europhys. Lett.* 71(6), 918 (2005)
39. A. Widera, F. Gerbier, S. Fölling, T. Gericke, O. Mandel, and I. Bloch, Precision measurement of spin-dependent interaction strengths for spin-1 and spin-2 ^{87}Rb atoms, *New J. Phys.* 8(8), 152 (2006)
40. H. Schmaljohann, M. Erhard, J. Kronjäger, M. Kottke, S. van Staa, L. Cacciapuoti, J. J. Arlt, K. Bongs, and K. Sengstock, Dynamics of $F = 2$ Spinor Bose–Einstein condensates, *Phys. Rev. Lett.* 92(4), 040402 (2004)
41. T. Kuwamoto, K. Araki, T. Eno, and T. Hirano, Magnetic field dependence of the dynamics of ^{87}Rb spin-2 Bose–Einstein condensates, *Phys. Rev. A* 69(6), 063604 (2004)
42. X. T. Xu, Z. Y. Wang, R. H. Jiao, C. R. Yi, W. Sun, and S. Chen, Ultra-low noise magnetic field for quantum gases, *Rev. Sci. Instrum.* 90(5), 054708 (2019)
43. B. Merkel, K. Thirumalai, J. E. Tarlton, V. M. Schäfer, C. J. Ballance, T. P. Harty, and D. M. Lucas, Magnetic field stabilization system for atomic physics experiments, *Rev. Sci. Instrum.* 90(4), 044702 (2019)
44. F. Riehle, Frequency Standards: Basics and Applications, Wiley-VCH Verlag GmbH & Co. KGaA, Weinheim, 2004
45. H. C. J. Gan, G. Maslennikov, K. W. Tseng, T. R. Tan, R. Kaewuam, K. J. Arnold, D. Matsukevich, and M. D. Barrett, Oscillating-magnetic-field effects in high-precision metrology, *Phys. Rev. A* 98(3), 032514 (2018)